Universiteit
Leiden
The Netherlands

# To IMAGE or to IMAGINE: visualization of parasite migration as a means to support (malaria) parasite vaccine development

Korne, C.M. de

**Citation**
Korne, C. M. de. (2023, November 2). *To IMAGE or to IMAGINE: visualization of parasite migration as a means to support (malaria) parasite vaccine development*. Retrieved from https://hdl.handle.net/1887/3655877

| | |
|---|---|
| Version: | Publisher's Version |
| License: | Licence agreement concerning inclusion of doctoral thesis in the Institutional Repository of the University of Leiden |
| Downloaded from: | https://hdl.handle.net/1887/3655877 |

**Note:** To cite this publication please use the final published version (if applicable).

# To IMAGINE

## Part II

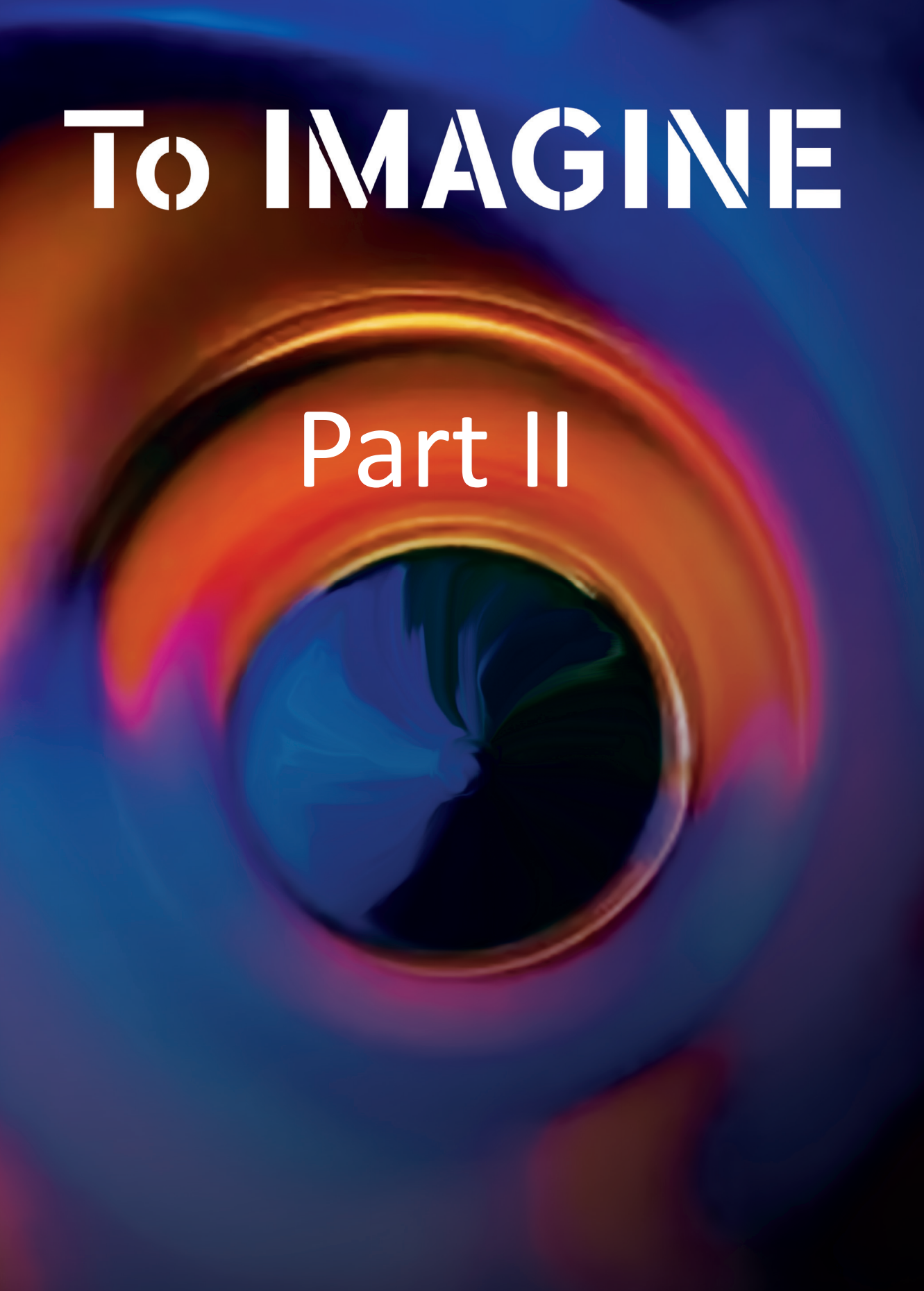


“
What is now proved was once only imagined.
- William Blake


6

# Development of a multimodal imaging setup to study human skin invasion by helminths

Clarize M. de Korne, Mick M. Welling, Danny M. van Willigen, Fabian W. Hensbergen, Meta Roestenberg, Fijs W.B. van Leeuwen

***Unpublished***

## ABSTRACT

In light of the continued global health threat posed by neglected tropical diseases such as helminths, there is a need for tools that can assist in the development of effective anthelminthic strategies. The aim of this study was to address this need by developing a multimodal imaging setup capable of visualizing and quantifying the invasion of human skin by *Schistosoma mansoni* and *Necator americanus* larvae. The hybrid tracer $^{99m}$Tc-Cy5-Methyl-AmineC4.MAS$_3$ was used, enabling the simultaneous fluorescent and radioactive labeling of the larvae and thereby facilitating the monitoring of their invasion patterns and the quantification of invasion events. This setup demonstrated the feasibility of a comprehensive and quantitative evaluation of helminthic invasion, offering opportunities for interventions aiming at obtaining a deeper understanding of the invasion process and serving as a useful readout for assessing the efficacy of future invasion-blocking strategies.

## INTRODUCTION

Schistosomiasis and hookworms are two of the most common neglected tropical diseases, currently affecting more than 10% of the world population. These parasitic infections cause chronic disease which a gradual decline in health (0.4 million life years and 2.2 million years of healthy life are lost annually) and eventually cause great economic impact[1]. Global control mainly relies on mass drug administration which has reduced overall disease morbidity, but due to drug-failure and high re-infection rates in endemic areas, schistosomiasis and hookworm infection have remained a global health threat[2].

Schistosomes and hookworms are skin-invading helminths; an infection starts when the infective larval stages of these helminths, which are free-living in water or soil, actively penetrate intact skin of their human host upon contact. Thereafter, the larvae migrate through the human body to the location suitable to mature into adult worms and to release eggs which are passed into the environment via the stool[3, 4]. Since the life cycles of these helminths depend amongst other things on the ability of the larvae to invade the skin, blocking skin invasion is one of the possible approaches to reduce disease transmission.

Despite being a crucial part of the life cycle and thereby a potential target for anthelminthic strategies, skin invasion by helminths has only rarely been studied. To date, only few studies using *in* vitro, rodent, canine or non-human primate models have provided some knowledge about the temporal dynamics of skin invasion and the key regulators, e.g. chemical cues, of the process[5-7]. These models have also been used to test several potential anti-penetrants, such as creams that act as a repellent/physical/larvicidal barrier or drugs that can kill larvae during the invasion process[8]. However, since the structure and composition of non-human skin differs significantly from that of human skin in terms of thickness, hairiness, and chemical properties[9-11] and the availability of large animal models for research is restricted, utilizing a human skin model would facilitate further investigation of helminthic skin invasion and assessment of potential invasion blocking strategies.

The limited use of a human skin model to study helminthic skin invasion can be attributed to the absence of an appropriate method to visualize and quantify invasion in human skin. Brightfield microscopy has been used to count and observe the behavior of helminths *in vitro*[3, 12, 13], however cannot be used to visualize helminths during skin invasion. On the other hand, molecular imaging techniques using fluorescent and radioactive labeling approaches have been successfully employed for *in vivo* studies of other pathogens (e.g. malaria parasites and *S. aureus* bacteria[14, 15]) as well as non-pathogenic cells (e.g. immune cells and stem cells[16, 17]). Thus, we reasoned that the development of a multimodal imaging setup for helminths would pave the way towards studying helminthic invasion in a human skin model.

We recently reported the preliminary results of monitoring skin invasion by schistosomes labeled with a fluorescent mitochondrial tracer[18]. In this study, we use the radiolabeled analogue $^{99m}$Tc-Cy5-Methyl-AmineC4.MAS$_3$ to label the larval stages of the helminths *Schistosoma mansoni* and *Necator americanus*. The fluorescent signature of the tracer was used to microscopically assess human skin invasion to deepen our understanding of that process. The radioactive signature was applied to establish a quantitative readout for helminthic skin invasion which may be useful in the future to assess the efficacy of potential parasite invasion blocking strategies.

## METHODS

### Parasite production

The Puerto Rican strain of *Schistosoma mansoni* (*Sm*) has been maintained in laboratory culture in the LUMC by means of its natural cycle between *B. glabrata* snails as the intermediate host and hamsters (RjHan:AURA strain; Janvier labs) as the definitive host as previously described[19]. To obtain larvae, infected snails were transferred to a 6-well plate filled with Bar-le-Duc water in a water bath at 30 °C. Subsequently, the snails were exposed to light and were allowed to shed larvae for 1 hr. Thereafter, the shed larvae were collected and kept at 30 °C until further use. Experiments were started within 1 hr after the collection of larvae. To count the larvae, 0.5 ml of the larvae solution was stained with Lugol's iodine and the stained larvae were counted using a stereomicroscope.

Third-stage larvae of *Necator americanus* (*Na*) were obtained from fecal samples collected from a healthy donor carrying a chronic hookworm infection (infected in the context of a controlled human hookworm infection trial[20]). The presence of *Na* eggs in the donor feces was confirmed by brightfield microscopy of Kato smears as described before[21]. Subsequently, 5 g feces was mixed with gentamicin (38 µl, stock: 40 mg/ml), amphotericin B (1 ml; stock: 750 µg/ml) and charcoal (1.5 g), placed on moist filter paper on a plastic platform in a petri dish and cultured for 7 days at 25 °C. Larvae migrated from the feces to the clean water surrounding the filter paper, were collected, washed and kept in Bar-le-Duc water at 25 °C until further use. The larvae were used up to 7 weeks after collection. The larvae were counted per 0.5 ml using a Leica M80 stereomicroscope (Leica Microsystems).

### Hybrid tracer synthesis

Cy5-AmineC4.MAS$_3$-Methyl was synthesized and characterized as described (see Chapter 6 from this thesis). In brief, the chelate mercaptoacetyltriserine (MAS$_3$) was coupled to Cy5-Methyl-AmineC4 by forming an amide bond, yielding the tracer Cy5- AmineC4.MAS$_3$-Methyl (from now abbreviated as Cy5-MAS$_3$). The crude compound was purified using preparative-scale prep-HPLC (high-performance liquid chromatography) and the product structure was confirmed by NMR (nuclear magnetic resonance) spectroscopy. Subsequently, the (photo)

physical properties of the tracer were assessed; the molar extinction coefficient (ε) and quantum yield (ΦF) were assessed to calculate the brightness (ε*ΦF) and the lipophilicity (log P) and serum binding were determined using methods previously described[22].

**Radiolabeling of Cy5-$MAS_3$**

Radiolabeling of Cy5-$MAS_3$ with technetium-99m was performed according to a previously described protocol (see Chapter 6 from this thesis) with some minor amendments. To Cy5-$MAS_3$, 1 GBq technetium-99m freshly eluted from a generator (~1 GBq/ml; Ultra-Technekow™, Mallinckrodt Medical B.V.) was added to a mixture containing 2.5 nmol of the tracer (992 µM stock in $H_2O$) and the following buffer solutions: 47.5 µl of phosphate buffer (0.5 M, pH 8), 50 µl of phosphate buffer (0.25 M, pH 8), 40 µl disodium tartrate dihydrate (50 mg/mL in phosphate buffer (0.5 M, pH 8)) and 10 µl of Tin(II) chloride dihydrate (4 mg/ml in L-ascorbic acid solution (3 mg/ml in 0.1 M HCl)) (Sigma-Aldrich). The Tin(II) chloride dihydrate solution was freshly prepared and $N_2$ degassed for 20 min, all other buffers were prepared and stored at 4°C for maximally 1 month. After heating the reaction mixture to 100°C for 20 min, the reaction mixture was cooled down to room temperature and diluted with 10 ml Milli-Q water. This solution was passed through a Sep-Pak C-18 cartridge (Waters) pre-rinsed with EtOH, followed by another 10 ml of Milli-Q water. After that, the labeled tracer was drop-wise eluted from the cartridge with EtOH into the reaction tube followed by vigorous vortexing. The volume of this eluate was reduced to 5 µl by evaporation of ethanol. The radiochemical purity of the final product $^{99m}$Tc-Cy5-$MAS_3$ was analyzed by radio-thin layer chromatography (radio-TLC; Supelco) using acetonitrile as mobile phase and the identity of the final product was confirmed using a HPLC system (high-performance liquid chromatography; Waters).

**Parasite labeling**

To label the *Sm* larvae with Cy5-$MAS_3$ (for fluorescent-based read-out) or $^{99m}$Tc-Cy5-$MAS_3$ (for radioactivity-based readout), 2.5 nmol tracer in 5 µl EtOH was added to 495 µl of the larvae in Bar-le-Duc water. The larvae were incubated for 1 hr at 31 °C and subsequently washed. To wash the larvae, 4.5 ml of Bar-le-Duc water was added to the labeling solution and the 5 ml larvae solution was added to the reservoir of an überStrainer (filter mesh size 10 µm; Pluriselect). The strainer was connected to a valve which allowed to control the filter flow rate and to prevent the filter from running dry during the wash steps. The larvae were washed twice by draining and refilling the reservoir with Bar-le-Duc water and subsequently the reservoir was connected to a peristaltic pump (flow rate 1.3 l/hr; Gilson) for 30 minutes.

To label the *Na* larvae with Cy5-$MAS_3$ (for fluorescent-based read-out) or $^{99m}$Tc-Cy5-$MAS_3$ (for radioactivity-based readout), 2.5 nmol tracer in 5 µl EtOH was added to 1245 µl of the larvae in Bar-le-Duc water. The larvae were incubated for 3 hr at 25 °C and subsequently

washed. To wash the larvae, the larvae solution was poured through a pluriStrainer (filter mesh size 10 µm; Pluriselect) followed by 500 ml Bar-le-Duc water. Subsequently, the larvae were collected from the filter and the wash step was repeated.

**Parasite labeling stability**

To determine the stability of the labeling of *Sm* and *Na* larvae over time, at various intervals up to 24 hr after labeling, larvae labeled with $^{99m}$Tc-Cy5-MAS$_3$ were filtered (Millex-HV syringe filter unit, 0.2 µm; Millipore). Subsequently, the radioactivity in the filtrate was measured with a gamma counter (Wizard2 2470 automatic gamma scintillation counter; PerkinElmer) and compared to the amount of radioactivity in a non-filtered sample to calculate the percentage decrease of parasite-bound tracer.

**Parasite viability and labeling toxicity**

The viability of the *Sm* larvae was assessed by brightfield microscopy; the number of whole larvae and separated larval bodies and tails were counted as well as moving and non-moving larvae. The viability of the *Na* larvae was also assessed by brightfield microscopy; moving and non-moving larvae were counted after stimulation with water of 50°C. After labeling of the *Sm* and *Na* larvae with $^{99m}$Tc-Cy5-MAS$_3$, their viability was confirmed before further use. To determine possible toxic effects of $^{99m}$Tc-Cy5-MAS$_3$, the viability of labeled and non-labeled *Sm* and *Na* larvae was assessed over time, at various intervals up to 48 hr after labeling. Brightfield movies of the *Sm* and *Na* larvae in solution were captured using a Leica AF6000 inverted widefield microscope with a 1.25x objective (Leica Microsystems). Using the Fiji package for the open-source software ImageJ[23] the movies were compressed into a single image using minimum-intensity projection (retrieves the level of minimum intensity over time for each x,y position).

**Fluorescence-based imaging of skin invasion**

Human skin explants were obtained from collaborating surgery centers immediately after cosmetic mastectomy. The use of human skin explants for this research was approved by the Commission Medical Ethics (CME) of the LUMC (CME: B18-009). The methods were carried out in accordance with the relevant guidelines and regulations, and informed consent was obtained from all participants. Pieces of human skin (5 x 10 mm) were placed into a confocal dish (Ø35mm; MatTek Corporation). The fluorescently labeled *Sm* larvae were added to the epidermal side of the skin piece and invasion was imaged using a Leica TCS (true confocal scanning) SP8X WLL (white light laser) microscope with a 10x objective (Leica Microsystems). Cy5-MAS$_3$ was excited at 633 nm and the emission was collected between 650 and 700 nm. The UV-laser (excitation: 405 nm, emission: 420–470 nm) was used to visualize the skin structures based on its autofluorescence. The movies were recorded with a frame rate of 70 frames per minute. The fluorescently labeled *Na* larvae were added to a piece of gauze (Ø 10

mm; Cutisoft) which was placed in a confocal dish. A piece of skin (10 x 10 mm) was, with the epidermal side down, put on top of the gauze. Movies of the *Na* larvae were captured using a Leica AF6000 inverted widefield microscope with a 10x objective (Leica Microsystems). Cy5-$MAS_3$ was excited at 633 nm and the movies were recorded with a frame rate of 240 frames per minute. Images with a higher resolution of the empty sheaths of the *Na* larvae were taken with a Leica TCS SP8X WLL microscope with a 40x objective (Leica Microsystems).

**Radioactivity-based assessment of skin invasion**

Pieces of human skin explant (~2x2 cm) were pre-heated to 37 °C before exposing them to *Sm* or *Na* larvae. The skin was exposed for 30 min to *Sm* larvae by putting a piece of skin on top of a well (24-well plate; Greiner Bio-One) filled with Bar-le-Duc water containing different numbers of radiolabeled larvae depending on the larval batch. Dose was normalized per experiment as a percentage of the highest dose. A plastic insert was used to allow the skin to be in contact with the solution without falling into it. The skin was exposed for 1 hr to 20, 40 or 60 *Na* larvae by putting a piece of skin on top of a piece of gauze (3x3 cm) containing radiolabeled larvae. To control for the radioactivity counts resulting from the presence of unbound tracer, control skin pieces were exposed to the last flow-through obtained during the washing of the *Sm* or *Na* larvae. During exposure, the skin was kept warm by putting a heating element at 37 °C on top of the skin. After exposure, the skin was rinsed with Bar-le-Duc water and counted using a gamma counter (Wizard2 2470 automatic gamma scintillation counter, Perkin Elmer).

**Statistical analysis**

The average and variability of the data were summarized using the mean and standard deviation (SD). The correlation between two numeric variables was assessed using the Pearson's correlation coefficient. p-values of <0.05 were considered significant. All statistical tests were performed by SPSS Statistics (IBM Nederland BV).



## RESULTS

**Development of a hybrid tracer labeling approach**

A hybrid tracer suitable to label the helminth larval stages was developed by coupling a previously synthesized fluorescent mitochondrial tracer Cy5-Methyl-Methyl[24] to a $MAS_3$ chelate followed by $^{99m}$Tc radiolabeling. The resulting hybrid tracer $^{99m}$Tc-Cy5-$MAS_3$ was used to label *Sm* larvae freshly shed by their snail intermediate host and *Na* larvae cultured from donated feces from a controlled hookworm infection trial participant (Figure 1AB). The radiolabeling of Cy5-$MAS_3$ with $^{99m}$Tc yielded 78 ± 9% binding of the total added radioactivity. The brightness of the tracer was $3.45 \cdot 10^3$ $M^{-1} \cdot cm^{-1}$ (the product of its quantum yield $\phi_{F, PBS}$ = 13% and molar extinction coefficient $\varepsilon_{PBS} = 2.65 \cdot 10^4$ $M^{-1} \cdot cm^{-1}$). A filter set-up was developed to purify the labeled larvae from the unbound tracer while preserving their viability (Figure

1C). Since *Sm* larvae are known to transform when exposed to high water turbulence or die when taken out of the water, this was prevented by controlling the flowrate in the filter set-up to allow for slow continuous washing. By filtering, >99.99% of the unbound tracer could be removed, reducing the background signal from the solution to <3% for *Sm* larvae and <1% for *Na* larvae (Figure 1D). Microscopical examination of the labeled *Sm* and *Na* larvae revealed that the larvae were wholly labeled; their outer membrane as well as their internal organs were labeled (Figure 1E-F).

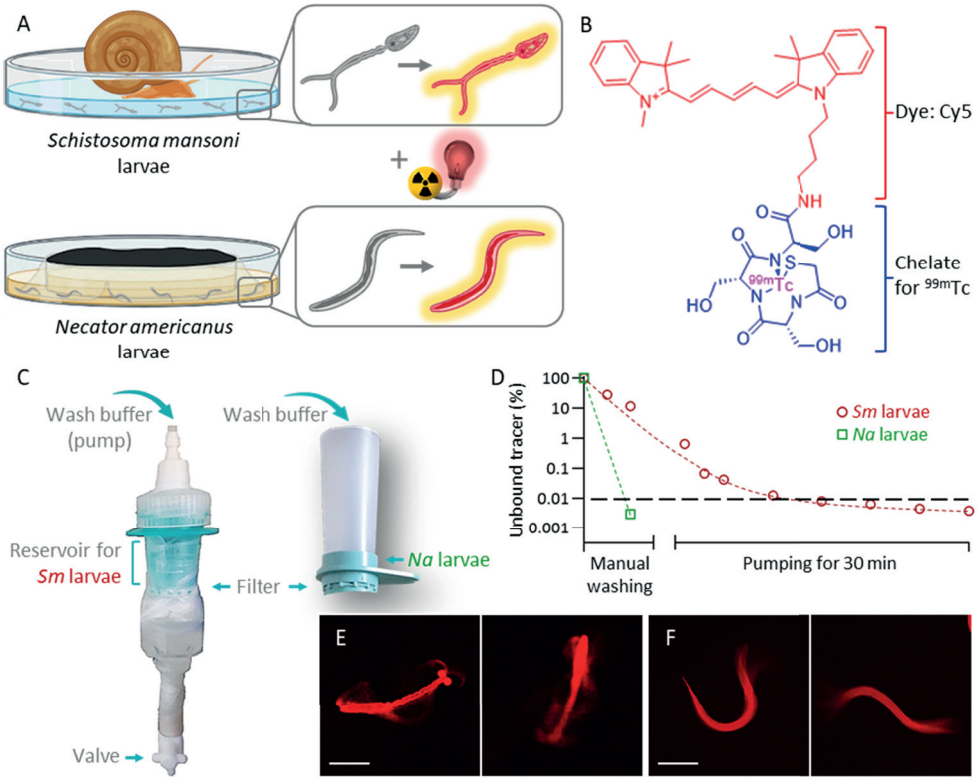


**Figure 1 Hybrid tracer labeling approach for helminthic larvae.** A) The *Schistosoma mansoni* (*Sm*) larvae were shed by their intermediate snail host and the *Necator americanus* (*Na*) larvae were cultured from feces containing eggs. The larvae were labeled with a hybrid tracer. B) The chemical structure of the hybrid tracer $^{99m}$Tc-Cy5-Methyl-AmineC4.MAS$_3$ which contains a Cy5 dye (depicted in red) and a MAS$_3$ chelate (depicted in blue) containing $^{99m}$Tc (depicted in pink). C) The filter set-up for *Sm* and *Na* larvae based on the use of a filter with a mesh size of 10 µm. D) Quantification of the reduction of the percentage of unbound tracer by filtering. E-F) Microscopic analysis of *Sm* (E) and *Na* larvae (F) labeled with the Cy5-MAS$_3$ tracer (shown in red). Scale bar: 150 µm.

**Labeling stability and parasite viability over time**

The stability of the labeling was assessed by measuring the reduction in the percentage bound tracer *in vitro*. Four hours after labeling, the time frame in which the labeled larvae were used for experiments, still >80% of the tracer was bound to the larvae (Figure 2A). The viability of the larvae was assessed by counting the percentage of motile larvae (Figure 2CD). In solution, the *Sm* larvae displayed intermittent backward (tail-first) locomotion by beating their tails (Figure 2C). The *Na* larvae propagated sinusoidal waves along their bodies, but this movement did not result in forward or backward locomotion (Figure 2D). The viability of the labeled larvae directly after the labeling procedure was comparable to unlabeled larvae; 99 ±1 % of the *Sm* larvae were viable and 93 ± 3% of the *Na* larvae (Figure 2B-D). Over time, the viability of the *Sm* larvae decreased which was independent of the labeling (viability at t=24 hr: 69 ± 8 %) (Figure 2B). The viability of the *Na* larvae did not decrease over the measured period of time (viability at t=48 hr: 93 ± 5%) (Figure 2B).

**Microscopic assessment of skin invasion behavior**

The labeling method was subsequently used to assess the skin invasion behavior of helminth larvae. The larvae were exposed to human skin explants in a set-up suited for confocal microscopic analysis (Figure 3A). The *Sm* larvae approached the skin in a body-first swimming mode (Figure 3B). Within minutes, the larvae were able to penetrate the skin. Three different ways of skin invasion were observed: 1) larvae penetrated the skin with their head, the head got separated from the tail and continued migration through the skin while the tail was left behind, 2) larvae penetrated the skin completely and whether or not shed their tail while migrating through the skin (some larvae disappeared from the field of view before they had shed their tail), 3) larvae penetrated the skin with their head but no further migration was observed during the observed period of time (Figure 3B).

The *Na* larvae were not able to propel forward in an aqueous environment (Figure 2D), however a structured environment better mimicking their natural soil environment, enabled 3-dimensional locomotion (Figure 3C). Therefore, the *Na* larvae were exposed to human skin while present in gauze. Unlike the *Sm* larvae, the gauze limited the visualization of *Na* larvae while penetrating. However, upon skin exposure, exsheathment could be observed (Figure 3C).

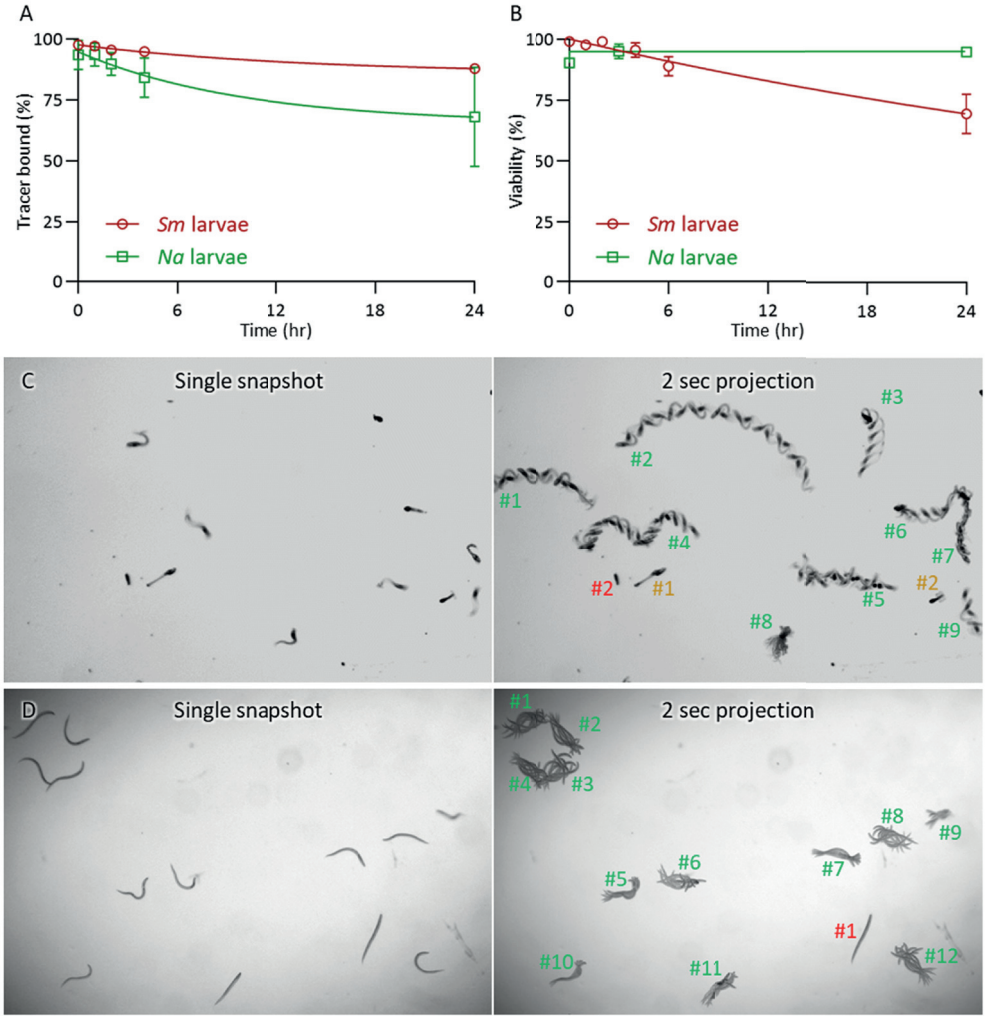


**Figure 2 Labeling stability and parasite viability.** A) The stability of the labeling plotted as the percentage of tracer bound to *Sm* and *Na* larvae over time. B) The viability of labeled *Sm* and *Na* larvae plotted as the percentage of motile larvae over time. C) A single brightfield image of *Sm* larvae (left) and a minimum intensity projection of the single brightfield image including the 19 consecutive frames captured in 2 s (right). The moving larvae are annotated in green, the stationary larvae are annotated in orange, the fallen apart larvae are annotated in red. D) A single brightfield image of *Na* larvae (left) and a minimum intensity projection of the single brightfield image including the 9 consecutive frames captured in 2 s (right). The moving larvae are annotated in green, the stationary larvae are annotated red.

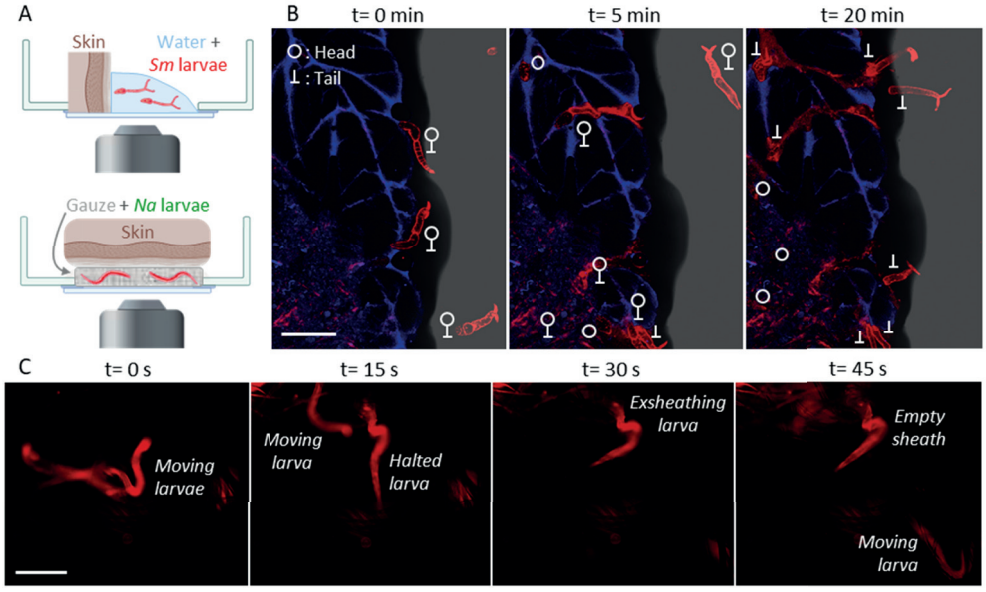


**Figure 3 Microscopic assessment of skin invasion behavior.** A) Schematic overview of the imaging set-up to monitor skin invasion behavior of *Sm* and *Na* larvae. B) Three screenshots from a movie (t=0, 5, 20 min) of skin-invading *Sm* larvae are shown; the brightfield signal is shown in grey, labeled larvae are shown in red and autofluorescence signal from the skin is shown in blue. The (separated) heads (O) and tails (⊥) of the larvae are annotated. Scale bar: 250 µm. C) Four screenshots from a movie (t=0, 15, 30, 45 s) of skin-exposed *Na* larvae in gauze are shown; labeled larvae are shown in red. Scale bar: 200 µm.

### Radioactivity-based quantification of skin invasion

The radioactivity signature of the hybrid tracer was used to quantify skin invasion by *Sm* and *Na* larvae. Human skin was exposed to radiolabeled *Sm* larvae in solution or *Na* larvae in gauze (Figure 4A). Subsequently, the radioactivity signal in the skin was quantified. For both exposure to *Sm* and *Na* larvae, the radioactivity retrieved from the skin was linearly correlated with the amount of larval exposure (Pearson's correlation coefficient *Sm* larvae: 0.951, *Na* larvae: 0.958; $p<0.001$) (Figure 4DE). Skin invasion was confirmed by microscopic assessment of the remaining larval solution and gauze. Mainly separated tails from the *Sm* larvae and empty sheaths from the *Na* larvae were found back (Figure 4B-C).

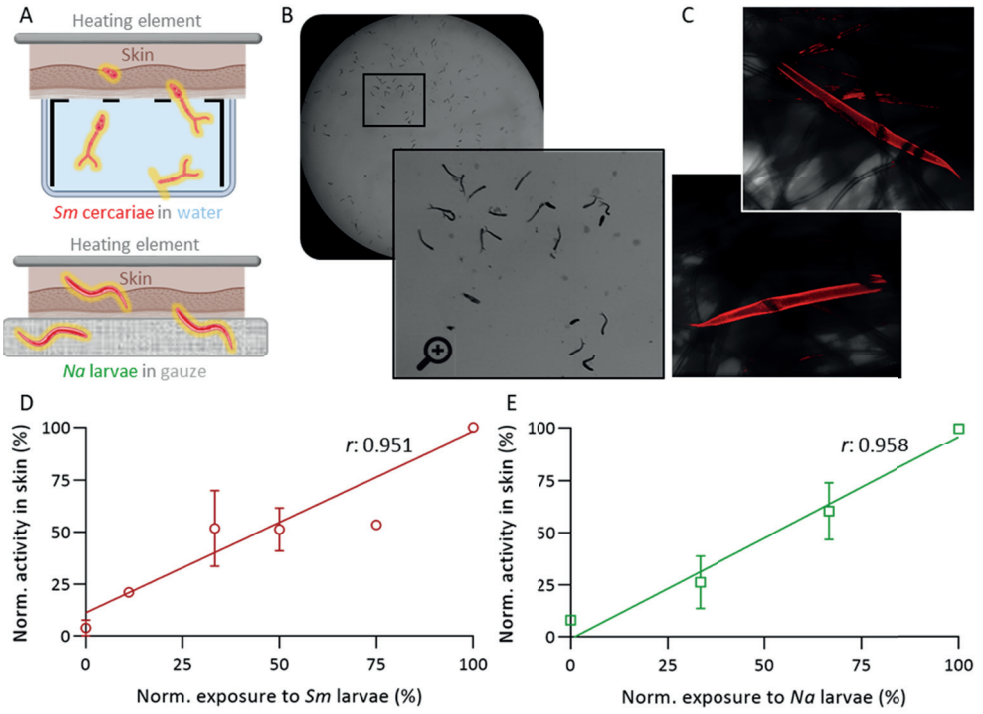


**Figure 4 Radioactivity-based quantification of skin invasion.** A) Schematic overview of the set-up to quantify skin invasion by *Sm* and *Na* larvae. B) The *Sm* larvae solution after skin exposure, mainly containing separated tails. C) Empty sheaths of *Na* larvae (depicted in red) in gauze after skin exposure. D) Quantification of skin invasion by *Sm* larvae. The radioactivity retrieved from the skin is plotted against the exposure to *Sm* larvae, normalized to the maximum dose. Pearson's correlation coefficient: 0.951; p<0.001. E) Quantification of skin invasion by *Na* larvae. The radioactivity retrieved from the skin is plotted against the exposure to *Na* larvae, normalized to the maximum dose. Pearson's correlation coefficient: 0.958; p<0.001.

## DISCUSSION

In this study we present a multimodal imaging setup to study human skin invasion of helminths using the hybrid tracer $^{99m}$Tc-Cy5-MAS$_3$. The fluorescent signature of the tracer allowed for real-time microscopical assessment of *Schistosoma mansoni* (*Sm*) and *Necator americanus* (*Na*) larvae invading human skin explant. The radioactive signature provided a quantitative measurement of the extent of skin invasion by *Sm* and *Na* larvae; we found that the radioactivity retrieved from the skin was directly proportional to the number of larvae in the exposure solution. This assay can aid investigating skin invasion by helminths and evaluating potential anti-invasion strategies aimed at preventing the neglected tropical diseases caused by these parasites.

Labeled *Sm* and *Na* larvae formed the basis of this study. Uniquely, we had both human

helminth species at our disposal, since the *Sm* life cycle has been maintained in laboratory culture in the LUMC and *Na* larvae could be obtained from a donor participating in a controlled human hookworm infection trial[19, 20]. The limited availability of larvae for research in non-endemic areas, as well as the limited options for labeling them endogenously (expression of reporter proteins) or exogenously (use of imaging agents), have resulted in a paucity of imaging studies focused on helminths[25-28]. The use of the hybrid tracer $^{99m}$Tc-Cy5-MAS$_3$ was successful in labeling both *Sm* and *Na* larvae for *ex vivo* imaging, while preserving their viability. This offers the prospect of a widely applicable exogenous labeling strategy for helminths that can advance further imaging-based research.

This study and our recent study using the precursor of the hybrid tracer used here (Cy5-Methyl-Methyl[18]) are the first to report real-time monitoring of human skin invasion by schistosomes. Prior studies on helminth behavior 1) have limited real-time monitoring to *in vitro* setups[13, 29-31], 2) mainly relied on animal models for *in/ex vivo* invasion studies[32-34] and 3) were based on retrospective assessment to estimate (human skin) invasion[35, 36]. The integration of these aspects in a single setup enhances the comprehensive study of host-seeking and invasion behavior, leading to the acquisition of complementary information. For instance, previous studies have reported both tail-first and head-first swimming patterns of schistosomes[12]. However, our integrated setup emphasized the role of skin in regulating these swimming patterns, as head-first swimming was observed during invasion and tail-first swimming occurred in the absence of skin. Moreover, as a follow-up to the discovery of delayed tail loss by Whitfield *et al.* that challenged the widely accepted notion that larvae immediately lose their tails upon skin penetration[37], our assay enables further exploration of this process by real-time monitoring of its temporal and spatial dynamics which may have immunological consequences. In case of the *Na* larvae, incorporating a transparent material that allows for movement, rather than the non-transparent gauze used in this study, would facilitate real-time monitoring of their complete human skin invasion. Incorporating a motility analysis tools into the setup may add value by providing detailed information about the motility patterns of these larvae[15, 38-40].

The radiolabeling approach provided a quantitative evaluation of the invasion of *Sm* and *Na* larvae. The need for a quantitative readout to assess the anthelminthic properties of potential new drugs and invasion blockers has been acknowledged in the field, as several screening assays have been recently developed[41-45]. Our radiolabeling approach offered a more direct and quantitative measurement of the efficacy of invasion blockers as opposed to the more indirect measures utilized thus far such as the effect on *in vitro* motility of larvae and adult worms or, in the case of *Sm* larvae, the count of released tails as a proxy for transformation. In the past, metabolic radiolabeling has been applied to study the distribution and migration patterns of schistosomes within rodent host tissue[46, 47]. However, up to

now there were no radiotracers available suitable for tracking of live helminths[26]. To improve the accuracy of the quantification, a filtering setup was developed that reduced the background signal while maintaining the larvae viability, resulting in a sufficient signal-to-background ratio. Further standardization of the setup is required to progress from the relative quantification of invasion applied in this study to a quantification of the absolute number of invaded larvae.

In conclusion, our study introduced a novel multimodal imaging approach that combined fluorescent and radioactive imaging to assess helminth skin invasion in real-time using a human skin explant model. This setup enables a more comprehensive and quantitative evaluation of helminthic invasion, providing possibilities for gaining deeper insights into this process as well as serving as a useful readout for assessing the efficacy of future helminth invasion-blocking strategies.

**Acknowledgments:** We are grateful to our colleagues Jacqueline Janse, Yvonne Kruize and Jan Pieter Koopman and the anonymous donor, for their assistance in obtaining the *Necator americanus* larvae through fecal donation. We also extend our gratitude to Jan de Best, Arifa Ozir-Fazalalikhan and Jeroen Sijtsma for their support in maintaining the life cycle of *Schistosoma mansoni* and providing the larvae. Furthermore, we would like to thank Leon Slof for providing building blocks used in the invasion assay. We acknowledge ChatGPT for providing assistance in generating written content during the preparation of this chapter.

## REFERENCES

1. Organization, W.H., Schistosomiasis and soil-transmitted helminthiases: progress report, 2020. Weekly Epidemiological Record= Relevé épidémiologique hebdomadaire, 2021. 96(48): p. 585-595.
2. Tsuji, N., Schistosomiasis and hookworm infection in humans: Disease burden, pathobiology and anthelmintic vaccines. Parasitology international, 2020. 75: p. 102051.
3. Chauhan, V.M., et al., The physicochemical fingerprint of Necator americanus. PLoS neglected tropical diseases, 2017. 11(12): p. e0005971.
4. Nation, C.S., et al., Schistosome migration in the definitive host. PLoS neglected tropical diseases, 2020. 14(4): p. e0007951.
5. Gang, S.S. and E.A. Hallem, Mechanisms of host seeking by parasitic nematodes. Molecular and biochemical parasitology, 2016. 208(1): p. 23-32.
6. McKerrow, J. and J. Salter, Invasion of skin by Schistosoma cercariae. Trends in parasitology, 2002. 18(5): p. 193-195.
7. Wheeler, N.J., E.A. Hallem, and M. Zamanian, Making sense of sensory behaviors in vector-borne helminths. Trends in Parasitology, 2022.
8. Downs, P.W., et al., New tools for the schistosomiasis elimination toolbox: Barriers and opportunities for the development of a topical cercarial anti-penetrant. 2017.
9. Jung, E.C. and H.I. Maibach, Animal models for percutaneous absorption. Topical drug bioavailability, bioequivalence, and penetration, 2014: p. 21-40.
10. Souci, L. and C. Denesvre, 3D skin models in domestic animals. Veterinary research, 2021. 52(1): p. 1-15.
11. Treuting, P.M., S.M. Dintzis, and K.S. Montine, Comparative Anatomy and Histology: A Mouse and Human Atlas. Academic Press, Elsevier, 2017. Chapter 24: p. 433-441.
12. Krishnamurthy, D., et al., Schistosoma mansoni cercariae swim efficiently by exploiting an elastohydrodynamic coupling. Nature Physics, 2017. 13(3): p. 266-271.
13. Nguyen, K., B. Gemmell, and J. Rohr, Effects of temperature and viscosity on miracidial and cercarial movement of Schistosoma mansoni: ramifications for disease transmission. International journal for parasitology, 2020. 50(2): p. 153-159.
14. Welling, M.M., et al., Multimodal Tracking of Controlled Staphylococcus aureus Infections in Mice. Acs Infectious Diseases, 2019. 5(7): p. 1160-1168.
15. Winkel, B.M.F., et al., Quantification of wild-type and radiation attenuated Plasmodium falciparum sporozoite motility in human skin. Scientific Reports, 2019. 9.
16. Perrin, J., et al., Cell tracking in cancer immunotherapy. Frontiers in Medicine, 2020. 7: p. 34.
17. Roca, M., et al., Guidelines for the labelling of leucocytes with 111In-oxine. European journal of nuclear medicine and molecular imaging, 2010. 37(4): p. 835-841.
18. Winkel, B.M.F., et al., Early Induction of Human Regulatory Dermal Antigen Presenting Cells by Skin-Penetrating Schistosoma Mansoni Cercariae. Frontiers in Immunology, 2018. 9.
19. Janse, J.J., et al., Establishing the production of male Schistosoma mansoni cercariae for a controlled human infection model. The Journal of infectious diseases, 2018. 218(7): p. 1142-1146.
20. Hoogerwerf, M.-A., et al., New insights into the kinetics and variability of egg excretion in controlled human hookworm infections. The Journal of infectious diseases, 2019. 220(6): p. 1044-1048.
21. Meurs, L., et al., Diagnosing polyparasitism in a high-prevalence setting in Beira, Mozambique: detection of intestinal parasites in fecal samples by microscopy and real-time PCR. PLoS neglected tropical diseases, 2017. 11(1): p. e0005310.
22. Hensbergen, A.W., et al., Evaluation of asymmetric orthogonal cyanine fluorophores. Dyes and Pigments, 2020. 183: p. 108712.
23. Schindelin, J., et al., Fiji: an open-source platform for biological-image analysis. Nat Methods, 2012. 9(7): p. 676-82.
24. Winkel, B.M.F., et al., A tracer-based method enables tracking of Plasmodium falciparum malaria parasites during human skin infection Theranostics, 2019. 9(10): p. 2768-2778.
25. Beckmann, S. and C. Grevelding, Paving the way for transgenic schistosomes. Parasitology, 2012. 139(5): p. 651-668.
26. de Korne, C.M., et al., Imaging as a (pre) clinical tool in parasitology. Trends in Parasitology, 2023.

27. Novobilsky, A. and J. Hoglund, Small animal in vivo imaging of parasitic infections: A systematic review. Experimental Parasitology, 2020. 214.
28. Pearce, E. and J. Lok, Imaging trematode and nematode parasites. Parasite Immunology, 2013. 35(9-10): p. 248-255.
29. Bryant, A.S., et al., A critical role for thermosensation in host seeking by skin-penetrating nematodes. Current Biology, 2018. 28(14): p. 2338-2347. e6.
30. Santos, M.J., et al., Qualitative and quantitative behavioral traits in a community of furcocercariae trematodes: tools for species separation? Journal of Parasitology, 2007. 93(6): p. 1319-1323.
31. Selbach, C. and R. Poulin, Parasites in space and time: a novel method to assess and illustrate host-searching behaviour of trematode cercariae. Parasitology, 2018. 145(11): p. 1469-1474.
32. Krautz-Peterson, G., et al., Imaging schistosomes in vivo. The FASEB Journal, 2009. 23(8): p. 2673.
33. Paveley, R.A., et al., Fluorescent imaging of antigen released by a skin-invading helminth reveals differential uptake and activation profiles by antigen presenting cells. PLoS neglected tropical diseases, 2009. 3(10): p. e528.
34. Pellegrino, J., Protection against human schistosome cercariae. Experimental Parasitology, 1967. 21(1): p. 112-131.
35. Cooper, E., et al., A comparison of topical formulations for the prevention of human schistosomiasis. Journal of pharmacy and pharmacology, 2004. 56(8): p. 957-962.
36. Ingram, R., et al., Dimethicone barrier cream prevents infection of human skin by schistosome cercariae: evidence from Franz cell studies. Journal of Parasitology, 2002. 88(2): p. 399-402.
37. Whitfield, P., et al., Delayed tail loss during the invasion of human skin by schistosome cercariae. Parasitology, 2003. 126(2): p. 135-140.
38. Ramot, D., et al., The Parallel Worm Tracker: a platform for measuring average speed and drug-induced paralysis in nematodes. PloS one, 2008. 3(5): p. e2208.
39. Storey, B., et al., Utilization of computer processed high definition video imaging for measuring motility of microscopic nematode stages on a quantitative scale:"The Worminator". International Journal for Parasitology: Drugs and Drug Resistance, 2014. 4(3): p. 233-243.
40. de Korne, C., et al., Clustering and erratic movement patterns of syringe-injected versus mosquito-inoculated malaria sporozoites underlie decreased infectivity. Msphere, 2021. 6(2): p. e00218-21.
41. Bartlett, A., et al., The infection of human skin by schistosome cercariae: studies using Franz cells. Parasitology, 2000. 121(1): p. 49-54.
42. Duguet, T.B., et al., Identification of annotated bioactive molecules that impair motility of the blood fluke Schistosoma mansoni. International Journal for Parasitology: Drugs and Drug Resistance, 2020. 13: p. 73-88.
43. Kotze, A., et al., An in vitro larval motility assay to determine anthelmintic sensitivity for human hookworm and Strongyloides species. The American journal of tropical medicine and hygiene, 2004. 71(5): p. 608-616.
44. Tritten, L., O. Braissant, and J. Keiser, Comparison of novel and existing tools for studying drug sensitivity against the hookworm Ancylostoma ceylanicum in vitro. Parasitology, 2012. 139(3): p. 348-357.
45. Wangchuk, P., et al., Identification of lead chemotherapeutic agents from medicinal plants against blood flukes and whipworms. Scientific reports, 2016. 6(1): p. 32101.
46. Li, J.-W., et al., Tran35S-labeling of cercariae of Schistosoma mansoni: a less expensive tool for tracing in vivo migration of schistosomula in mice. Parasitology International, 1997. 46(1): p. 55-65.
47. Salafsky, B., et al., Evaluation of N, N-diethyl-m-toluamide (DEET) as a topical agent for preventing skin penetration by cercariae of Schistosoma mansoni. The American journal of tropical medicine and hygiene, 1998. 58(6): p. 828-834.